ADVANCED FUNCTIONAL MATERIALS
www.afm-journal.de

Collective Organization Behaviors of Multi-Cell Systems Induced by Engineered ECM-Cell Mechanical Coupling

Xiaochen Wang, Hangyu Li, Yu Zheng, Dongshi Guan, Aidan Wang, Qihui Fan, Yang Jiao,* and Fangfu Ye**

Cells in vivo are surrounded by fibrous extracellular matrix (ECM), which can mediate the propagation of active cellular forces through stressed fiber bundles and regulate various biological processes. However, the mechanisms for multi-cellular organization and collective dynamics induced by cell-ECM mechanical couplings, which are crucial for the development of novel ECM-based biomaterial for cell manipulation and biomechanical applications, remain poorly understood. Herein, the authors design an in vitro quasi-3D experimental system and demonstrate a transition between spreading and aggregating in collective organizational behaviors of discrete multi-cellular systems, induced by engineered ECM-cell mechanical coupling, with the observed phenomena and underlying mechanisms differing fundamentally from those of cell monolayers. During the process of collective cell organization, the collagen substrate undergoes reconstruction into a dense fiber network structure, which is correlated with local cellular density and consistent with observed enhanced cells' motility; and the weakening of fiber bundle formation within the hydrogel reduces cells' movement. Moreover, cells can respond to the curvature and shape of the original cell population and form different aggregation patterns. These results elucidate important physical factors involved in collective cell organization and provide important references for potential applications of biomaterials in new therapies and tissue engineering.

1. Introduction

Collective cell behaviors are fundamental to various biological processes, including tissue formation, wound healing, immune response, and cancer cell invasion.[1–4] Cells work together to perform specific tasks, such as dividing, migrating, and recognizing, through various communication mechanisms like chemical signals, electrical impulses, and mechanical interactions.[3,5–8] In these processes, the ability of cells to sense and respond to mechanical signals is critical, as it plays a vital role in maintaining tissue homeostasis and enabling adaptation to environmental changes.[9–15]

In vivo, cells are surrounded by the extracellular matrix (ECM), which provides structural support and transmits mechanical signals.[16,17] The ECM can be deformed, stretched, or stiffened due to mechanical forces exerted by cells, yielding changes in the ECM microstructure. These changes can be sensed by cells through integrins, focal adhesions, and cytoskeletal elements.[18–20] The collagen fibers between adjacent cells can be

X. Wang, F. Ye
Oujiang Laboratory (Zhejiang Lab for Regenerative Medicine, Vision and Brain Health)
Wenzhou Institute
University of Chinese Academy of Sciences
Wenzhou 325000, China
E-mail: fye@iphy.ac.cn

X. Wang, Q. Fan, F. Ye
Beijing National Laboratory for Condensed Matter Physics
Institute of Physics
Chinese Academy of Sciences
Beijing 100190, China
E-mail: fanqh@iphy.ac.cn

X. Wang, F. Ye
School of Physical Sciences
University of Chinese Academy of Sciences
Beijing 100049, China

H. Li, D. Guan
State Key Laboratory of Nonlinear Mechanics
Institute of Mechanics
Chinese Academy of Sciences
Beijing 100190, China

H. Li, D. Guan
School of Engineering Science
University of Chinese Academy of Sciences
Beijing 100049, China

Y. Zheng, Y. Jiao
Materials Science and Engineering
Arizona State University
Tempe, AZ 85287, USA
E-mail: yang.jiao.2@asu.edu

Y. Zheng, Y. Jiao
Department of Physics
Arizona State University
Tempe, AZ 85287, USA

A. Wang
Aidi School
Beijing 100018, China

The ORCID identification number(s) for the author(s) of this article can be found under https://doi.org/10.1002/adfm.202305414

DOI: 10.1002/adfm.202305414

significantly reorganized and remodeled to form thick fiber bundles that are very effective force carriers, leading to strongly correlated migration of the cells.[19,21–24] Recently, the force-guided motion of single cells has been demonstrated to be critically dependent on ECM-mediated force transmission.[25–27] The ECM, therefore, mediates mechanical signaling between cells that do not directly contact each other, regulating the cells' collective behaviors and maintaining tissue integrity.[21]

ECM remodeling is critical for many biological processes, such as tissue development, wound healing, and tissue repair.[2,18] Despite the recent progress in understanding ECM-mediated force transmission in regulating individual cell dynamics, how the ECM-cell mechanical coupling can give rise to a distinct spectrum of collective dynamics and multi-cellular organizational behaviors is not well understood.

Here, we demonstrate a transition in collective organizational behaviors of multi-cellular systems induced by cell-ECM mechanical coupling. This is achieved by designing an in vitro quasi-3D experimental system and seeding discrete cell populations on different substrates, thereby altering the nature of cell-substrate coupling. By investigating time-lapse images and tracking cells' trajectories, we observed a well-defined spreading-aggregating transition in a simple convex-shaped cell population, when the solid substrate is replaced by the collagen hydrogel. From the displacement field of collagen, we find that individual cell contraction forces combine to form a centripetal force field, which guides cell motions during the aggregation process. Interestingly, we also observe a non-trivial dependence of the aggregation behavior on the curvature of the original cell population's boundary. For example, in the case of a "round wound pattern" (a concentric ring structure with a hollow center), strong contraction forces transmitted via the fiber bundles between circumferentially adjacent cells led to a collective centripetal migration near the wound boundary. In contrast, in the case of a "straight wound pattern" with parallel edges between two cell populations, cells would not close the "wound", but migrate towards opposite directions.

During collective cell organization, the collagen substrate was reconstructed into a dense fiber network structure, correlated with local cellular density and consistent with observed enhanced cells' motility, providing further evidence for collagen-induced intercellular attraction and resulting collective dynamics. When the fiber bundle formation is weakened within the hydrogel associated with a low gelation temperature, the cell movements also reduce. By studying ECM-mediated mechanical coupling and collective cell motion regulated by collagen hydrogel, we obtained results that not only contribute to fundamental biophysical research but also have implications for new therapies and tissue engineering. The study provides valuable insights into the importance of mechanical signals in regulating collective cell behavior, as well as the potential functions of ECM remodeling in tissue regeneration and engineering.

2. Results

2.1. Collagen Substrate Induces Collective Cell Aggregation

We developed an in vitro experimental system to investigate the regulation of the collective behavior of discrete cell populations (i.e., initially non-contacting individual cells) by the extracellular matrix. We aim to regulate cells' collective behaviors by introducing contraction force transmitted through ECM. To accomplish this, we seeded discrete cell populations consisting of human mammary gland epithelial cells (MCF10A), each population with ≈2000 μm in size, on the substrate of either the Petri dish or the collagen I hydrogel (**Figure 1**a).

Compared to the solid substrate, the collagen I hydrogel is a non-linear elastic fibrous material and a major ECM component in vivo, which can generate long-range mechanical signal propagation by changing the local stiffness gradient and microstructure.[9,18] We seeded cells on the solid substrate (Petri dish) within a polydimethylsiloxane (PDMS) chamber. One hour after the cells' attachment, we removed the confining chamber, and the cells spread randomly, causing the cell population to expand outward (Figure 1c). In contrast, we introduced the 2 mg mL^{-1} collagen I hydrogel to create a quasi-3D experimental system and deposited the cells directly on the top of the collagen. Strikingly, the cell population started retracting, decreasing in size, and eventually forming a dense cell assembly after 17 h (Figure 1e and Figure S1, Supporting Information).

When the substrate is changed, cell migration mode changes from spreading to aggregating, referred to as a transition in cells' collective behaviors. In contrast to previous active models that focus on the spreading process of cell monolayers,[28] our quasi-3D experimental system consists of discrete cells without direct force transmission through adhesive cell junctions. However, it is discovered that cells can also transmit mechanical signals by deforming the collagen substrate. We know from previous studies that cells can restructure collagen during migration, and the reorganized collagen bundle can carry tensile forces, significantly enhancing intercellular interactions.[25] Therefore, as the solid substrate was changed to collagen hydrogel, the cellular dynamic transitioned from random motion to collective migration (Figure 1i), prompting us to explore the mechanisms underlying this correlated motion.

To measure the collagen displacement field of this quasi-3D experimental system, we pre-mixed fluorescent micro-beads (0.8 μm in diameter) in collagen and quantified the displacements of micro-beads by the particle image velocimetry (PIV) analysis technique. As the cell population aggregated, the cells generated radial inward-pointing tractions (Figure 1g). When a single cell is on the collagen surface, it generates a force field centered around the cell through its contraction. If the cell population is arranged in a circular pattern on the collagen surface, the forces from individual cells are coupled together to form a centripetal force field toward the center of the collagen substrate (Figure 1g). This force field had already existed at the initial moment, and the average speed of cells at the same location was larger than adjacent beads within ECM (Figure S2, Supporting Information), proving that the cell population continued to move under the guidance of the centripetal force field.

We recorded cells' migration using time-lapse inverted microscopy and confocal microscopy at 10-min intervals for 6 h. We tracked the trajectories of cells on 2D and quasi-3D substrates and calculated the velocities (Figure 1d,f). The random migration of cells on the solid substrate could be regarded as a diffusion during the 6 h of observation. In contrast, cells seeded on collagen exhibited clear collective migration toward the center of the population. To characterize the spatial distribution of cells' movement,

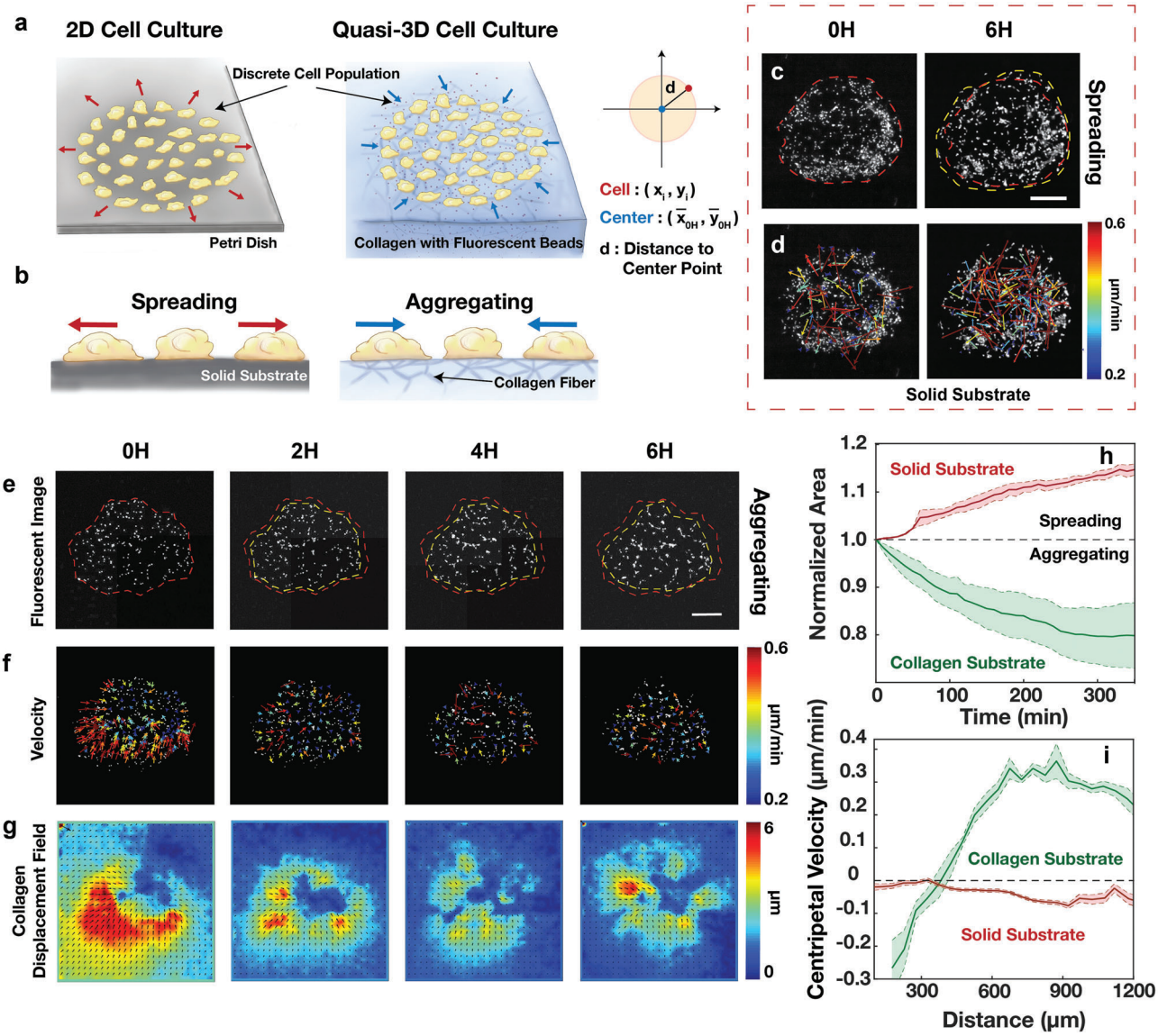

Figure 1. Collagen substrate induces cell collective aggregation. a,b) Schematic of 2D (left) and quasi-3D (right) in vitro system with discrete cell populations. c,d) On the Petri dish, the cell population expands outward with random velocities. On top of fibrous collagen hydrogel, the cell population retracts and decreases in size. e) Phase contrast images (red dashed line: cell population boundary at 0 h), f) cells' velocity, and g) collagen displacement field with 10-min intervals for "round pattern" cell population with a size of 2000 μm on the collagen substrate. h) Evolution of cell population size and i) spatial distribution of the centripetal velocity. Data are presented as mean ± SEM. $n > 500$ data points. The scale bars are 500 μm.

we calculated each cell's location and centripetal velocity relative to the center. A positive centripetal velocity indicates that the cells move toward the center, while a negative velocity indicates cell migration in an outward direction. We defined the central point as the average coordinates of all cells' positions at the initial time. On the solid surface, the centripetal velocities of cells are negative and do not vary with distance, indicating uniform outward diffusion. However, on collagen substrate, the average centripetal velocity of cells is larger than 0 and positively correlated with distance. The velocity of cells located more than 900 μm away shows a slight decrease. Within the range of 350 μm, the centripetal velocities of cells are negative, because as approaching the center the selection of the center point significantly influences the centripetal velocity direction. During the aggregation process, the center points constantly change, leading to an imprecise definition of centripetal velocity.

2.2. Boundary Curvature Influences Cells' Organizational Behavior

Human tissues and organs have complex and varied shapes, and the deformation of cell populations in response to different geometric boundaries remains an important area of investigation.[29,30] To explore this relationship, we altered the shape of cell populations by using PDMS masks to create straight

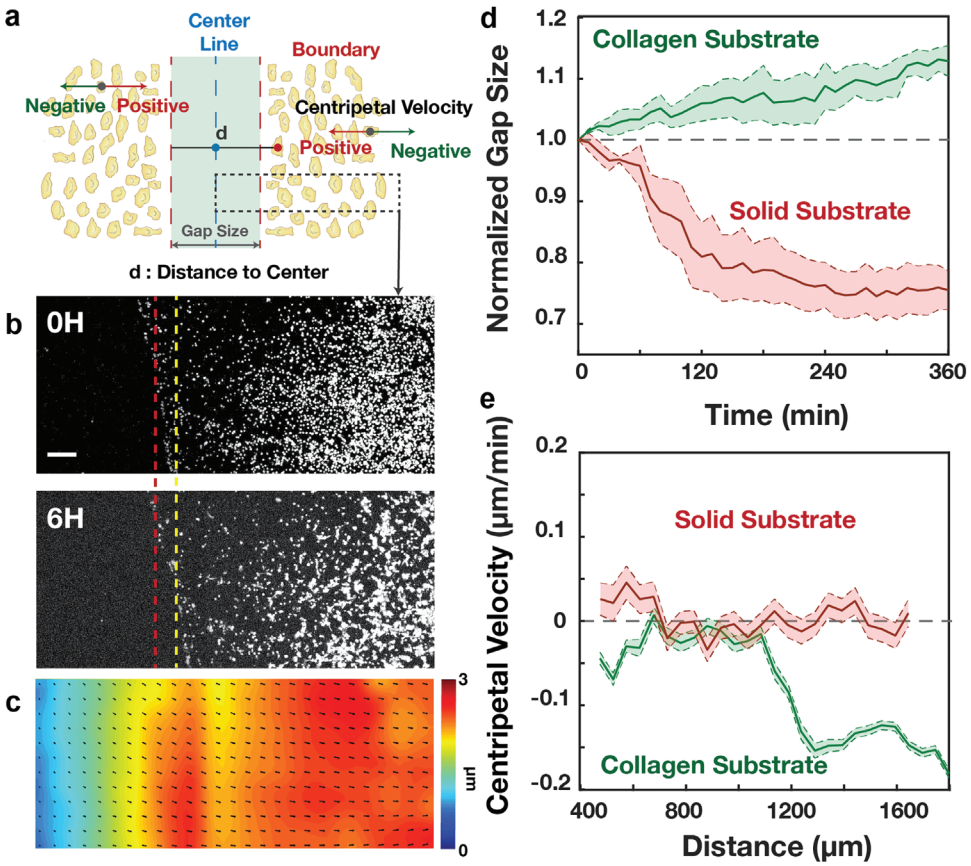

Figure 2. Collective aggregation of cell population with straight boundary. a) Illustration of the discrete cell population with a straight boundary. b) On the top of collagen hydrogel, the cell population aggregates with the boundary right shifting (red: 0 h, yellow: 6 h). c) Average displacement field of the collagen substrate in 6 h. d) Evolution of the gap size and e) spatial distribution of the centripetal velocity . Data are presented as mean ± SEM. $n > 500$ data points. The scale bar is 200 μm.

or concave curved boundaries. We measured the velocity component of cells along the normal direction of the boundary to characterize their collective motion relative to the central positions, with positive values indicating contraction and negative values indicating expansion.

In the cell populations with straight boundaries (**Figure 2**a), cells exhibit random migration on solid substrates, and the boundary shifts towards the cell-free area with the gap size decreases (Movie S6, Supporting Information). However, when seeded on top of collagen, the cell population contracts and the gap size increases within 6 h (Figure 2d). The cell populations also undergo a transition from spreading to aggregating. Analysis of the average collagen displacement fields shows that a constant force field coupling between the cells population was approximately perpendicular to the boundary. Therefore, when the boundary curvature ≥ 0, the coupling force fields point towards the interior of the cell population along the normal direction of the boundary on the top of collagen.

Then, we further investigate the collective cell behaviors with negative curvature boundaries, by constructing a hollow geometric structure of cell populations. For solid substrates, we covered PDMS masks (≈2000 μm in size) on a Petri dish and seeded cells around them, then removed the PDMS masks to create a hollow structure. Because the PDMS masks would destroy the surface structure of collagen hydrogels, we injected a bubble with a diameter of about 1500 μm onto the collagen substrate and added the cell suspension around it to create the hollow cell pattern. After cells had adhered to the collagen substrate, the bubble was removed.

We used time-lapse microscopy to track the cells' trajectories and calculate the size of the "wound area" over time. The coordinates of the entire cell population were converted into a polar coordinate system, with the origin set as the center of the wound. The entire pattern was divided into 36 regions, each spanning a 10° interval. We used the "Boundary" and "Polyarea" functions in the MATLAB toolbox to obtain the area of the region enclosed by the boundary of the cell population. The tracking results indicate that the wounds on collagen hydrogel shrink faster than those on solid substrates (**Figure 3**f).

At the initial time point after cell seeding (0 h), the traction forces of cells on the collagen substrate in the region far from the wound boundary are coupled to form a centripetal displacement field, with the displacement increasing with distance (Figure 3e and Figure S3, Supporting Information). However, the collagen displacement field was in the centrifugal direction near the boundary. As the cell population shrinks, the direction of the collagen displacement field near the wound boundary gradually changes to a centripetal direction (Figure S4, Supporting

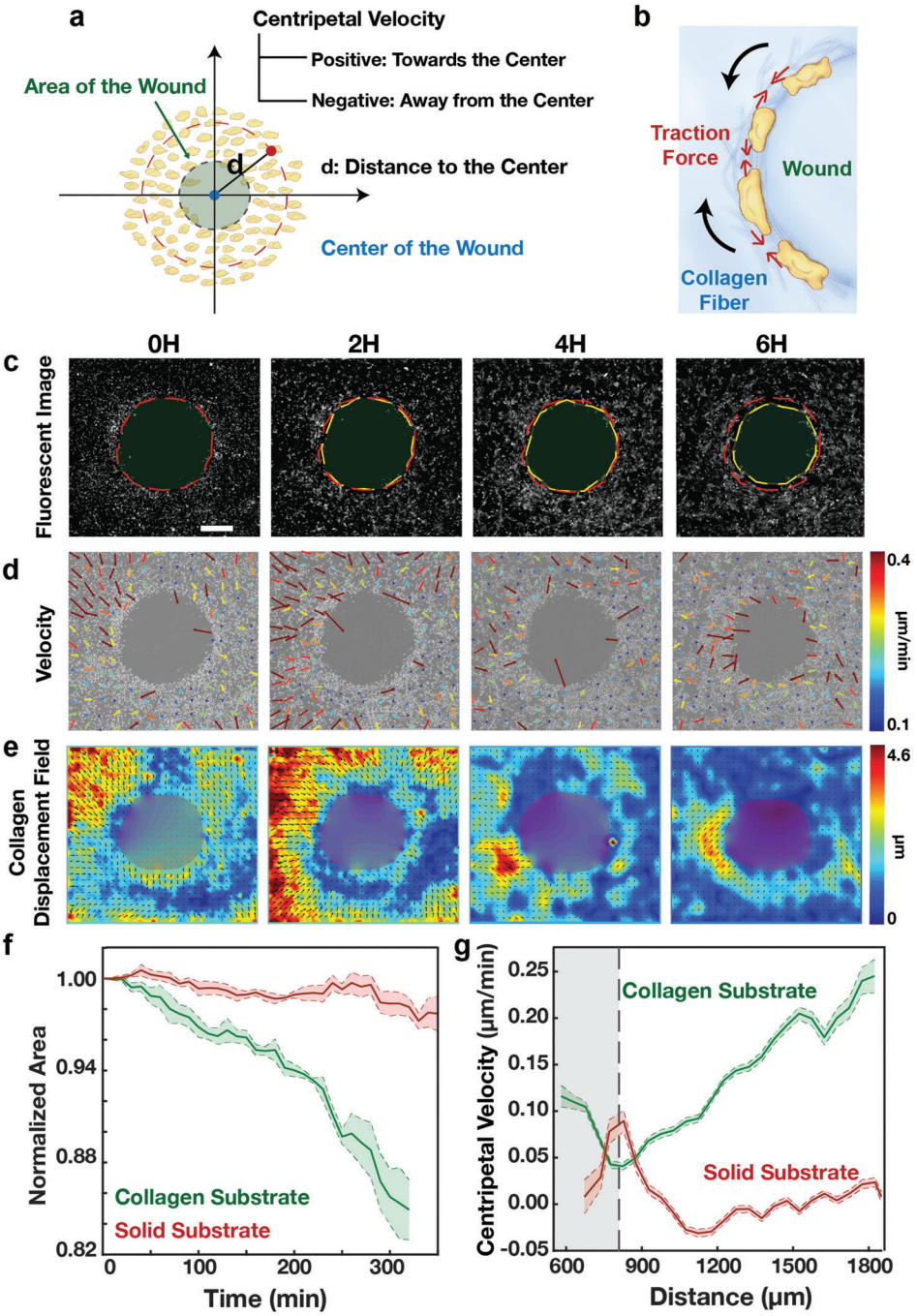

Figure 3. Collective aggregation of cell population with "wound pattern". a) Schematic of the discrete cell population with a "wound pattern". b) Illustration of traction forces transited by collagen fiber bundles at the wound boundary. On the top of fibrous collagen hydrogel, the cell population aggregates toward the center and the wound decreases in size. c) Phase contrast images (red dashed line: wound boundary at 0 h), d) cells' velocity, and e) collagen displacement field with 10-min intervals for "wound pattern" cell population with a diameter of 1500 μm on the collagen substrate. f) Evolution of the wound size and g) spatial distribution of the centripetal velocity (gray area: cells near the boundary) on different substrates. Data are presented as mean ± SEM. $n > 500$ data points. The scale bar is 400 μm.

Information). To characterize the spatial distribution of cell motion, we calculated the centripetal velocity v and location d (distance to the wound center). The cells' centripetal velocity is positive, and the distribution could be divided into two parts: 1) Far from the wound boundary ($d > 825$ μm, right side of the dotted line), the velocity is positively proportional to the distance, similar to the aggregation pattern of cells with a positive curvature boundary; 2) Near the wound boundary ($d < 825$ μm, left side of the dotted line), the centripetal velocity is inversely proportional to the distance (Figure 3g). The aggregation of cells

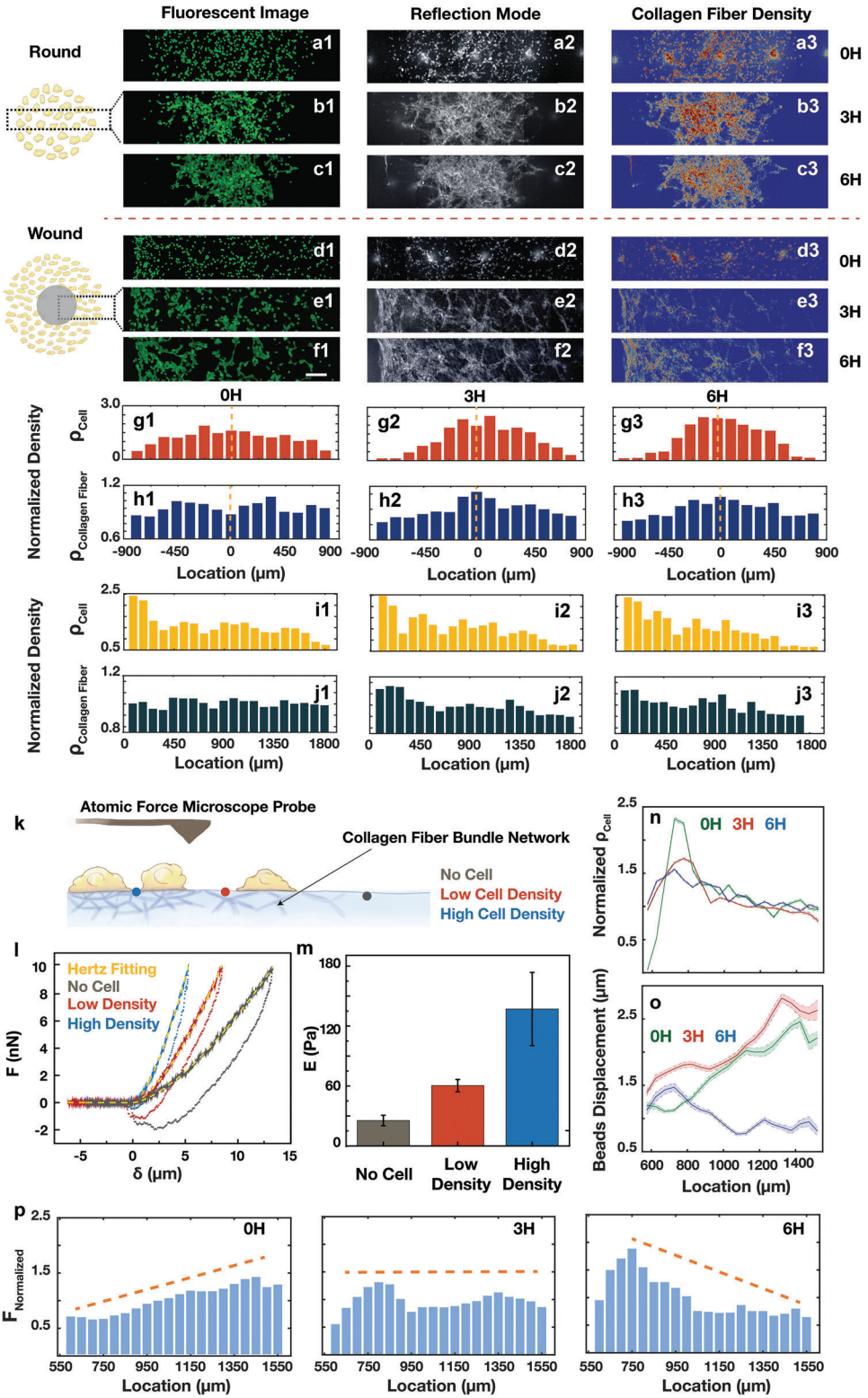

Figure 4. Re-organized fiber bundle network induces cellular collective aggregation. a1–c1) Fluorescent images, a2—c2) collagen fiber images recorded under the reflection mode, and a3–c3) map of collagen fiber density for a selected area of the "round pattern" cell population (dashed box means the location of the selected area). d1—f1) Fluorescent images, d2—f2) collagen fiber images recorded in reflection mode, and d3—f3) map of collagen fiber density for a selected area of the "wound pattern" cell population (dashed box means the location of the selected area) (the scale bar is 200 μm). g–j) The evolution of the spatial distributions of cells' density and collagen fiber in g,h) "round pattern" and i,j) "wound pattern" cell population. k) Schematic of the mechanical measurement using AFM. l) Force-indentation curves measured on the collagen gel at three different regions: no cell (black curve),

near the wound boundary appeared to be due to the strong attraction between circumferentially adjacent cells, coupling into a centripetal force that resembled the effect of surface tension.

2.3. Re-Organized Fiber Bundle Network Regulates Collective Aggregation

Previous studies have shown that cells can re-organize collagen fibers to form thick fiber bundles parallel to the connecting cell centers. These re-organized fiber bundles transmit tension and induce strongly correlated migration of cells, which provides evidence for the collagen-matrix mediated attraction between cells.[25,26] Therefore, to investigate the mechanism behind the boundary-regulated aggregation behavior of MCF-10A cells on quasi-3D collagen hydrogel, we analyzed the collagen fibers around the cells using a laser scanning confocal microscope (SP8, Leica) in reflection mode.

Initially, collagen fibers are uniformly distributed surrounding cells. However, as shown in **Figure 4**a–f, aggregating cells pull and reshape collagen fibers to form a network of fiber bundles. As cell aggregation occurs, the density distribution of collagen fiber networks tends to match the cell density distribution. For "round shape" cell populations, collagen density decreases from the center to the boundary, resulting in a radial fiber bundle network (Figure 4a–c,g,h). For "wound pattern" cell populations, collagen density decreases from the inner edge of the cell cluster to the periphery, and the shape of the fiber bundle at the wound boundary is circumferential, indicating the strong attraction between circumferential neighboring cells and confirming the ECM-mediated centripetal force field (Figure 4d–f,i,j). It takes about 3 h of evolution for the collagen fiber bundles to form a circumferential structure. This verifies that the circumferential attraction between cells gradually increases during the cells' migration, so the collagen displacement field near the wound boundary changes from the centrifugal to the centripetal direction (Figure 4e). The co-localization of cells with collagen fiber bundles during cell population evolution indicates that the ECM-mediated mechanical couplings between migrating cells lead to collective migration dynamics. To further verify this mechanism, we perform ECM-field coupled active-particle simulations which explicitly take into account the cell-ECM mechanical feedback mechanism. The numerical results are in excellent agreement with the experimental observation, further confirming the proposed coupling effects (Section S3, Supporting Information).

Due to the remodeled fiber microstructure, the collagen substrate no longer has uniform mechanical properties, and the displacement field of collagen cannot directly characterize the force field. Therefore, we measured Young's modulus of collagen hydrogels with different microstructures by using atomic force microscopy (AFM).[31] After 3 h of cell population evolution on collagen substrates, the cell density distribution matches the collagen fiber bundle distribution. The high cell density corresponds to a high fiber concentration (Figure 4i2,i3,j2,j3). We characterized the elastic modulus of collagen with different cell densities in "wound pattern" cell populations after 6 h of evolution.

The AFM measurements were carried out in contact mode. The measured force–distance curves were recorded and fitted with Hertz model $F = \frac{4}{3(1-\upsilon^2)} E R^{0.5} \delta^{1.5}$ to calculate Young's modulus E,[32] where F is the measured force, R is the probe radius, δ is the indentation distance, and υ (=0.49) is the Poisson ratio.[33] Figure 4l shows the force-indentation curves measured on the collagen gel at three different regions: no cell, low cell density, and high cell density (Figure S5, Supporting Information). The indentation force $F(\delta)$ is measured as a function of indentation δ when the AFM probe first moves downward against the collagen surface (approach, solid lines) and then moves back away from the surface at the same speed (retract, doted lines). The yellow dashed lines show the fitting of the Hertz model to the approach curves. Figure 4m shows the variation of elastic modulus E in three different regions: no cell (25.48 ± 5.29 Pa), low cell density (60.35 ± 6.18 Pa), and high cell density (136.98 ± 36.64 Pa). It indicates that the region with dense collagen fiber bundle network has a higher elastic modulus.

Then, we used the mechanical properties of re-shaped collagen and the displacement field to estimate the distribution of traction forces during the evolution of the "wound pattern" cell population. Initially, the collagen fibers were uniformly distributed, and the traction force was proportional to the displacement of the beads mixed in collagen. As the cell population evolved, the elastic modulus of the collagen became positively related to the density of the fiber bundles (which could be indicated by the cell density). Therefore, the distribution of the traction force field was estimated as the joint product of the normalized cell density and the displacement of beads (Figure 4p). As the "wound pattern" cell population evolved on the collagen substrate, along the radial direction to the center, the distribution of the force field transitioned from decay to increase.

2.4. Effects of Collagen Microstructure and Universality of ECM-Cell Coupling Mechanism

The micromechanical properties of collagen gel are strongly influenced by its network architecture. The microstructure of collagen I can be modified by adjusting the gelation temperature, with higher temperatures resulting in a network composed of short and thin fibers, and lower temperatures leading to thicker fiber clusters.[34–36] As a general trend, the heterogeneity of the network decreases as temperature increases. To investigate whether the microstructure of the ECM can regulate the collective behavior of cells, we prepared a collagen I gel using a lower gelation temperature (21 °C) to serve as a substrate for the "wound pattern" cell population.

low cell density (red curve), and high cell density (blue curve). The indentation force $F(\delta)$ is measured as a function of indentation δ when the AFM probe first moves downward against the collagen surface at a constant loading speed $v = 10\ \mu m\ s^{-1}$ (approach, solid lines) and then moves back away from the surface at the same speed (retract, dotted lines). The yellow dashed lines show the fitting of the Hertz model to the approach curves with E = 21.04 Pa (no cell), 50.03 Pa (low cell density), and 103.85 Pa (high cell density). m) Variations of elastic modulus E in three different regions: no cell (25.48 ± 5.29 Pa, $N = 21$), low cell density (60.35 ± 6.18 Pa, $N = 41$), and high cell density (136.98 ± 36.64 Pa, $N = 84$). Data are presented as mean ± SD. The distributions of n) normalized cells' density, o) fluorescent beads' displacement, and p) the normalized estimated traction force at different times. Data are presented as mean ± SEM.

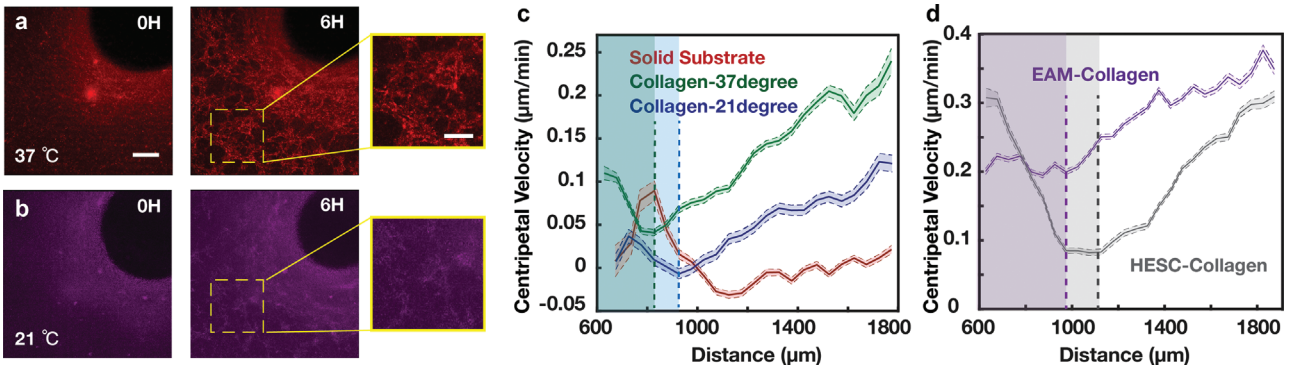

Figure 5. Cellular collective aggregation regulated by collagen microstructures and the collective migration of primary cell population. The evolution of the microstructure of the collagen fiber network re-organized by cells on the hydrogel with different gelation temperatures a) 37 and b) 21 °C, the scale bar is 200 μm. An enlarged view of the collagen fiber network is represented in the yellow box (the scale bar is 100 μm). c) Spatial distribution of the centripetal velocity of cells on different substrates (velocity of cells near the wound boundary are color labeled, green: 37 °C, blue: 21 °C). d) Spatial distribution of the centripetal velocity of primary cell population with "wound pattern" (velocity of cells near the wound boundary are color labeled, purple: EAM, gray: HESC).

We observed the cell population's evolution on low gelation temperature collagen substrate and recorded the microstructure of the collagen fiber network using confocal microscopy. Compared to the high gelation temperature collagen in previous tests (37 °C), the cell population weakly re-organizes the fiber network as the gelation temperature decreases to 21 °C. Even after 6 h of evolution, the collagen with low gelation temperature does not form thick bundles, and the circular collagen fiber bundles at the wound boundary are not visible (**Figure 5**b and Figure S6, Supporting Information). The spatial distributions of cell motion on collagen substrate with different gelation temperatures follow a similar shape (Figure 5c). However, as the temperature decreases, the overall centripetal velocities of cells also decrease. Therefore, when the cells cannot effectively reconstruct collagen to apply attractive forces, the collective movement of the cells becomes weaker. The microstructure of the collagen gel can change the local mechanical properties and significantly affect the re-organization of fiber bundles, which in turn regulates the collective behavior of cells (Figure S7, Supporting Information).

To further verify the collagen-regulated collective organization behaviors, we tested different types of primary cells, including primary endometriosis-associated macrophages (EAM) and primary endometrial stromal cells (human endometrial stromal cells, HESC). When the cells were seeded as a "wound pattern" on the high-gelation-temperature (37 °C) collagen, they also exhibited aggregative behaviors. Similar to the velocity spatial distribution of MCF10A cells, those of the two types of primary cells can also be divided into two parts. The centripetal velocities of the peripheral cells positively relate to the distance. In contrast, for the cells closer to the boundary of the wound, centripetal velocities decrease with distance (Figure 5d). Thus, the previously proposed cell aggregation mechanism is universal: the interaction between the outer cells is enhanced due to the attractive force mediated by collagen fibers, resulting in a centripetal force field; while at the inner concave boundary, cells are continuously attracted towards the center due to the stronger circumferential attraction between the cells mediated by collagen fiber bundles.

3. Discussion and Conclusion

We have demonstrated the significant role of ECM-cell mechanical coupling in regulating collective organizational behaviors of multi-cellular systems by unraveling a spreading-aggregating transition induced by collagen hydrogel. On the rigid substrate, the cell migration follows a random motion pattern as in traditional studies: when cells are seeded onto a substrate with a specific shape, they exhibit a tendency to spread freely from areas of higher cell density to regions of lower density due to the random diffusion and population pressure; as a result, the cell population displays an outward spreading behavior. Our study reveals that when cells are cultured on a collagen gel substrate with a "round pattern", the long-range mechanical coupling of individual migrating cells, transmitted by the collagen fiber network, breaks the symmetry of random cellular motion, and induces strong correlation. The individual cell contraction forces combine to form a centripetal force field, which guides a cell's motion translation from spreading to aggregating. In contrast, with a "wound pattern", strong contraction forces transmitted via fiber bundles between circumferentially adjacent cells cause collective centripetal migration near the concave boundary. Additionally, we demonstrate that fiber bundles formed due to the mechanical remodeling of the ECM by migrating cells can facilitate long-range force propagation in the ECM and regulate cell migration dynamics.

In epithelial monolayers or cell spheroids, intercellular adhesion, filamentous actin, and motor protein myosin II coordinate cell morphologies and collective migrations during tissue spreading and wound healing.[28,37–42] The ECM composition, viscosity, and rigidity regulate tissue spreading by affecting the orientation of actin stress fibers, cell migration mode, and cell-substrate interaction.[43] An active aggregating-spreading transition in cells' monolayer is characterized by modifications in cell-cell adhesion, cell-substrate adhesion, cell contractility, and substrate stiffness, resulting in the competition between traction forces and contractile intercellular stresses.[44] But in most experiments, the elastic modulus of soft polymer substrates is still higher than 1 kPa, and the linear elastic materials, such as polyacrylamide gels, could not accurately mimic the structural

remodeling and mechanics transmission of fibrous materials in vivo.[19,21,24,37] We emphasize that the strongly correlated long-range dynamic forces reported here, which govern the behavior of discrete cell populations, are transmitted through bundles of collagen fibers between individual cells rather than through intercellular adhesion as in previous studies on cell clusters.

Although recent research has highlighted the role of long-distance force in regulating tumor cell-immune cell interactions and collective invasion of cancer cells, the regulation of self-organization behaviors of cells population by intercellular mechanical signals remains poorly understood. To address this gap, we studied discrete cell populations in a quasi-3D model, which provided natural fibrous hydrogels as substrates to transmit force while avoiding the mechanical transfer generated by direct cell contact. Moreover, we quantified the correlation between cell dynamics, substrate displacement, and reshaped fiber bundle structure, providing direct experimental evidence for how the ECM mediates long-distance cell-cell interactions to regulate cell population behaviors. Similar behaviors are also observed in different types of cells, indicating that the cell collective motion triggered by collagen-mediated mechanical signaling follows a universal mechanism. Our results provide new insights into regulating cell population behavior in tissue engineering, organ repair, and other important biological processes. By identifying the mechanisms underlying the spreading-aggregating transition in cell populations with specific boundaries induced by collagen hydrogel, our study offers novel strategies for controlling cell population behavior in tissue engineering and regenerative medicine.

4. Experimental Section

Cell Culture and Labeling: The GFP-tagged normal human breast epithelial cell line MCF-10A cells (from the China Infrastructure of Cell Line Resource) were cultured in DMEM/F12 medium containing L-glutamine and 15 mM HEPES (10-092-CVR, Corning), supplemented with 5% horse serum (16050-122, Gibco), 1% penicillin/streptomycin (30-002-CI, Corning), 20 ng mL^{-1} human epidermal growth factor (PHG0311, Gibco), 10 µg mL^{-1} insulin (I-1882, Sigma), 100 ng mL^{-1} cholera toxin (C-8052, Sigma), and 0.5 µg mL^{-1} hydrocortisone (H-0888, Sigma).

The primary EAM and primary HESC were obtained from the laboratory of Prof. Ping Duan, the Second Affiliated Hospital of Wenzhou Medical University. EAMs were cultured in 1640 medium containing 10% FBS (Gibco) and 1% penicillin/streptomycin. HESCs were cultured in DMEM/F12 medium containing 10% FBS and 1% penicillin/streptomycin.

Cells were incubated at 37 °C with 5% CO_2. Trypsin (25-053-CI, Corning) and 1× PBS (46-013-CM, Corning) solution were applied to detach cells from the Petri dish. The cells were passaged every 5–6 days for a maximum of 20 passages. The primary cells were passaged for a maximum of 10 passages. 1 µL of calcein AM (Invitrogen) was diluted in 1 mL cell suspensions to fluorescently label primary cells. The cells were then incubated under the growth conditions for 30 min before a culture medium replaced the solution.

Collagen Gel Preparation: Type I collagen extracted from rat tail tendon (Corning) was diluted to a final concentration of 2 mg mL^{-1} and neutralized to pH ≈7 according to the product instructions. Collagen solution was added into a PDMS chamber (2 mm height), attached to the culture dish (Corning), and incubated at 37 °C for 30 min till gelation to form a collagen hydrogel substrate. For the quantitative characterization of the ECM displacement, fluorescent microbeads (Sphero) with a diameter of around 0.8 µm were pre-mixed into the collagen solution, then uniformly embedded in the matrix as displacement markers after collagen gelation. The collagen solution was incubated at room temperature to get the collagen I gel with a lower gelation temperature.

Cell Patterning on Solid or Collagen Substrate: For the "round pattern" cell populations on a solid substrate, 300 cells were added in PDMS chambers (diameter of 2 mm), which were placed on the Petri dishes. One hour later, the cells attached to the substrate and the PDMS chamber were removed. When the substrate was replaced by the collagen matrix, a 0.5 µl drop containing ≈300 cells was placed on top of the gels. After the cells were attached, the culture medium was added to cover the samples.

In the case of "wound pattern" cell populations on Petri dishes, the PDMS was cut into circles with a diameter of 2 mm and attached to the dishes. The cells were seeded around the PDMS with ≈4×10^4 cells per mL. For the cells on collagen, a bubble (with a diameter of about 1500 µm) was injected onto the collagen substrate, and 5 µl the cell suspension (5×10^6 cells per mL) was added around it. After cells adhered to the substrate, the PDMS mask or bubbles were removed, and more medium was added. The formation of the cell population's straight boundary was masked by a PDMS strip.

Imaging and Cell Tracking: Inverted fluorescent microscopy (Nikon Ti-E) and confocal microscopy (Leica SP8) were used to acquire 2D and 3D time-lapse images (10× Objective lens). The microscopes worked with live-cell incubating systems, which could maintain the culture condition (37 °C, 5% CO_2) for more than 24 h. The time interval was 10 min. The reflection mode of the confocal microscopy was used to capture collagen-fiber microstructures (25X Water-immersion Objective Lens). The 3D multi-channel raw images were projected into 2D images with ImageJ (NIH). Software Imaris was used to track the time-dependent positions of the centroids of individual cells.

Analysis of ECM Displacement Fields: The fluorescent beads mixed in the collagen hydrogel were dynamically tracked with the confocal microscope for 6 h. The 3D images were projected into 2D images using ImageJ. The collagen ECM displacement fields were analyzed by PIV lab software[45] based on the reference positions of the microbeads. Then the parameters of the collagen matrix displacement were quantitatively analyzed with MATLAB (MathWorks).

Analysis of Cell Density and Collagen Fiber Density: The confocal 3D reconstructed images were projected into 2D images using ImageJ. The gray value images were transferred into arrays. Along the *x*-axis, the images were separated into areas with a width of 400 pixels. The mean of gray value of each section was calculated to obtain a probability distribution of cells or collagen fibers.

AFM Setup and Operation: Hydrogel force indentation measurements were performed using an AFM (MFP-3D, Asylum Research) with a colloidal probe. The AFM was set up on an inverted microscope (IX71, Olympus) equipped with an EMCCD camera (Ixon3, Andor). The colloidal probe consisted of a glass sphere of radius R (≅25 µm), glued on the front end of a rectangular cantilever beam (NSC35/Pt, MikroMasch) featuring a spring constant of 11 N/m. The freshly assembled colloidal probe was cleaned using a low-vacuum plasma cleaner (Harrick Plasma, PDC-32G) at the power of 40 W for 15 min. The vacuum level of the cleaner was kept at about 600 milli-torr during the plasma cleaning. The colloidal probe was then coated with a thin layer of poly(L-lysine)-graft-poly (ethylene glycol) (PLL-gPEG), which effectively reduced the adhesion of the hydrogel surface to the probe. Before each force measurement, the actual spring constant of the colloidal probe was calibrated in situ using the thermal power spectral density method. The AFM measurements were carried out in contact mode with F = 10 nN (≈5–15 µm indentation depths) and a constant loading speed $v = 10$ µm s^{-1}. All experiments were carried out at room temperature. Each force indentation measurement was performed at least five times to ensure the reproducibility and accuracy of the experiment results.

Supporting Information

Supporting Information is available from the Wiley Online Library or from the author.

Acknowledgements

The authors thank Yongliang Zhai of Soft Matter Lab for the design and fabrication of homemade live-cell incubating system. This work was supported by The National Key Research and Development Program of China (Grant No.2022YFA1405002, No.2020YFA0908200, and No.2021YFA0719302), the National Natural Science Foundation of China (Grants No. T2221001, No.12074407, No.12090054, and No.11972351), the Strategic Priority Research Program of Chinese Academy of Sciences (Grant No. XDB33030300), and The Youth Innovation Promotion Association of CAS (No. 2021007). Y.Z. and Y.J. have no financial support for this work.

Conflict of Interest

The authors declare no conflict of interest.

Author Contributions

Conceptualization: X.W., Q.F., Y.J., and F.Y., Methodology: X.W., H.L., and A.W., Investigation: X.W., H.L., D.G., Q.F., Y.J., and F.Y., Visualization: X.W. and H.L., Modeling and Simulation: Y.Z. and Y.J., Writing—original draft: X.W., H.L., D.G., Q.F., Y.J., and F.Y., Writing—review & editing: Q.F., Y.J., and F.Y.

Data Availability Statement

The data that support the findings of this study are available from the corresponding author upon reasonable request.

Keywords

biomaterials, cell organization, collagen, extracellular matrix, mechanical coupling

Received: May 16, 2023
Revised: June 8, 2023
Published online: July 7, 2023

[1] P. Friedl, D. Gilmour, *Nat. Rev. Mol. Cell Biol.* **2009**, *10*, 445.
[2] X. Trepat, E. Sahai, *Nat. Phys.* **2018**, *14*, 671.
[3] R. Basu, B. M. Whitlock, J. Husson, A. L.e Floc'h, W. Jin, A. Oyler-Yaniv, F. Dotiwala, G. Giannone, C. Hivroz, N. Biais, J. Lieberman, L. C. Kam, M. Huse, *Cell* **2016**, *165*, 100.
[4] R. Mayor, S. Etienne-Manneville, *Nat. Rev. Mol. Cell Biol.* **2016**, *17*, 97.
[5] I. Nitsan, S. Drori, Y. E. Lewis, S. Cohen, S. Tzlil, *Nat. Phys.* **2016**, *12*, 472.
[6] T. Zulueta-Coarasa, R. Fernandez-Gonzalez, *Nat. Phys.* **2018**, *14*, 750.
[7] X. Wang, S. Chen, H. Nan, R. Liu, Y. Ding, K. Song, J. Shuai, Q. Fan, Y. Zheng, F. Ye, Y. Jiao, L. Liu, *Research* **2021**.
[8] B. Ladoux, R. M. Mege, *Nat. Rev. Mol. Cell Biol.* **2017**, *18*, 743.
[9] A. Saraswathibhatla, D. Indana, O. Chaudhuri, *Nat. Rev. Mol. Cell Biol.* **2023**, *24*, 495.
[10] O. Chaudhuri, J. Cooper-White, P. A. Janmey, D. J. Mooney, V. B. Shenoy, *Nature* **2020**, *584*, 535.
[11] O. Chaudhuri, S. T. Koshy, C. Branco da Cunha, J.-W. Shin, C. S. Verbeke, K. H. Allison, D. J. Mooney, *Nat. Mater.* **2014**, *13*, 970.
[12] X.-B. Zhao, Y.-P. Chen, M. Tan, L. Zhao, Y.-Y. Zhai, Y.-L. Sun, Y. Gong, X.-Q. Feng, J. Du, Y.-B. Fan, *Adv. Healthcare Mater.* **2021**, *10*, 2100821.
[13] A. D. Doyle, N. Carvajal, A. Jin, K. Matsumoto, K. M. Yamada, *Nat. Commun.* **2015**, *6*, 8720.
[14] O. Chaudhuri, L. Gu, D. Klumpers, M. Darnell, S. A. Bencherif, J. C. Weaver, N. Huebsch, H.-p. Lee, E. Lippens, G. N. Duda, D. J. Mooney, *Nat. Mater.* **2016**, *15*, 326.
[15] M. Gómez-González, E. Latorre, M. Arroyo, X. Trepat, *Nat. Rev. Phys.* **2020**, *2*, 300.
[16] A. G. Clark, A. Maitra, C. Jacques, M. Bergert, C. Pérez-González, A. Simon, L. Lederer, A. Diz-Muñoz, X. Trepat, R. Voituriez, D. M. Vignjevic, *Nat. Mater.* **2022**, *21*, 1200.
[17] K. M. Yamada, M. Sixt, *Nat. Rev. Mol. Cell Biol.* **2019**, *20*, 738.
[18] J. S. Di Martino, A. R. Nobre, C. Mondal, I. Taha, E. F. Farias, E. J. Fertig, A. Naba, J. A. Aguirre-Ghiso, J. J. Bravo-Cordero, *Nat Cancer* **2022**, *3*, 90.
[19] M. S. Hall, F. Alisafaei, E. Ban, X. Feng, C.-Y. Hui, V. B. Shenoy, M. Wu, *Proc. Natl. Acad. Sci. USA* **2016**, *113*, 14043.
[20] Y. L. Han, P. Ronceray, G. Xu, A. Malandrino, R. D. Kamm, M. Lenz, C. P. Broedersz, M. Guo, *Proc. Natl. Acad. Sci. USA* **2018**, *115*, 4075.
[21] J. P. Winer, S. Oake, P. A. Janmey, *PLoS One* **2009**, *4*, 6382.
[22] P. Ronceray, C. P. Broedersz, M. Lenz, *Proc. Natl. Acad. Sci. USA* **2016**, *113*, 2827.
[23] Y. Zheng, Q. Fan, C. Z. Eddy, X. Wang, B. Sun, F. Ye, Y. Jiao, *Phys. Rev. E* **2020**, *102*, 052409.
[24] R. S. Sopher, H. Tokash, S. Natan, M. Sharabi, O. Shelah, O. Tchaicheeyan, A. Lesman, *Biophys. J.* **2018**, *115*, 1357.
[25] Q. Fan, Y. Zheng, X. Wang, R. Xie, Y. Ding, B. Wang, X. Yu, Y. Lu, L. Liu, Y. Li, M. Li, Y. Zhao, Y. Jiao, F. Ye, *Angew. Chem., Int. Ed.* **2021**, *60*, 11858.
[26] C. Yang, X. Wang, R. Xie, Y. Zhang, T. Xia, Y. Lu, F. Ye, P. Zhang, T. Cao, Y. Xu, Q. Fan, *Adv. Funct. Mater.* **2023**, *33*, 2211807.
[27] Y. Zheng, H. Nan, Y. Liu, Q. Fan, X. Wang, R. Liu, L. Liu, F. Ye, B. Sun, Y. Jiao, *Phys. Rev. E* **2019**, *100*, 043303.
[28] C. P. Heisenberg, Y. Bellaiche, *Cell* **2013**, *153*, 948.
[29] T. Chen, A. Callan-Jones, E. Fedorov, A. Ravasio, A. Brugués, H. T. Ong, Y. Toyama, B. C. Low, X. Trepat, T. Shemesh, R. Voituriez, B. Ladoux, *Nat. Phys.* **2019**, *15*, 393.
[30] J. James, E. D. Goluch, H. Hu, C. Liu, M. Mrksich, *Cell Motil.* **2008**, *65*, 841.
[31] D. Guan, Y. Shen, R. Zhang, P. Huang, P.-Y. Lai, P. Tong, *Phys. Rev. Res.* **2021**, *3*, 043166.
[32] B. H. Hertz, *J. Reine und angewandte Mathematik* **1882**, *92*, 156.
[33] A. P. G. Castro, P. Laity, M. Shariatzadeh, C. Wittkowske, C. Holland, D. Lacroix, *J. Mater. Sci.: Mater. Med.* **2016**, *27*, 79.
[34] J. Xie, M. Bao, S. M. C. Bruekers, W. T. S. Huck, *ACS Appl. Mater. Interfaces* **2017**, *9*, 19630.
[35] C. A. R. Jones, L. Liang, D. Lin, Y. Jiao, B. Sun, *Soft Matter* **2014**, *10*, 8855.
[36] C. A. R. Jones, M. Cibula, J. Feng, E. A. Krnacik, D. H. McIntyre, H. Levine, B. Sun, *Proc. Natl. Acad. Sci. USA* **2015**, *112*, E5117.
[37] G. Beaune, C. Blanch-Mercader, S. Douezan, J. Dumond, D. Gonzalez-Rodriguez, D. Cuvelier, T. Ondarçuhu, P. Sens, S. Dufour, M. P. Murrell, F. Brochard-Wyart, *Proc. Natl. Acad. Sci. USA* **2018**, *115*, 12926.
[38] G. Beaune, G. Duclos, N. Khalifat, T. V. Stirbat, D. M. Vignjevic, F. Brochard-Wyart, *Soft Matter* **2017**, *13*, 8474.
[39] S.-Z. Lin, B. Li, G.-K. Xu, X.-Q. Feng, *J. Biomech.* **2017**, *52*, 140.
[40] X. Wang, X. Xing, S. Lu, G. Du, Y. Zhang, Y. Ren, Y. Sun, J. Sun, Q. Fan, K. Liu, F. Wang, F. Ye, *Fundam. Res.* **2022**, https://doi.org/10.1016/j.fmre.2022.01.031.

[41] M. F. Staddon, M. P. Murrell, S. Banerjee, *Soft Matter* **2022**, *18*, 7877.
[42] S.-Z. Lin, S. Ye, G.-K. Xu, B. Li, X.-Q. Feng, *Biophys. J.* **2018**, *115*, 1826.
[43] S. Douezan, J. Dumond, F. Brochard-Wyart, *Soft Matter* **2012**, *8*, 4578.
[44] C. Pérez-González, R. Alert, C. Blanch-Mercader, M. Gómez-González, T. Kolodziej, E. Bazellieres, J. Casademunt, X. Trepat, *Nat. Phys.* **2018**, *15*, 79.
[45] T. William, R. Sonntag, *J. Open Res. Software* **2021**, *9*, 1.